JST: Engineering and Technology for Sustainable Development
Volume 34, Issue 3, July 2024, 039-046

Numerical Simulation of the Low-Reynold Flow through Tandem Circular Cylinders with the Middle Flat Plate

Van Tuyen Vu[1], Viet Dung Duong[2], Ich Long Ngo[1*]
[1]*Hanoi University of Science and Technology, Ha Noi, Vietnam*
[2]*Vietnam National University, Ha Noi, Vietnam*
[*]*Corresponding author email: long.ngoich@hust.edu.vn*

Abstract

The paper describes an investigation of the dynamic behaviors of the fluid flow through tandem circular cylinders with a middle flat plate. A low Reynold number of 100, which originated from appropriate applications, is considered. The Lattice Boltzmann Method is used and implemented in the Direct Numerical Simulation. The numerical model was well-validated by comparing results from the literature for either a single circular cylinder or two tandem cylinders without flat plates. Consequently, the dynamic behavior of the fluid flow through tandem circular cylinders with a middle flat plate is first revealed in this study. The numerical results show that these behaviors are affected significantly by the presence of the middle flat plate. Moreover, the pattern of vortex formation is also affected considerably when this flat plate is mounted between two cylinders, and this pattern changes at the threshold value of plate size. Hydrodynamic coefficients and the Strouhal number generally decrease with the increase in flat plate size. These results are very useful in reducing the losses caused by vortex formation and increasing the fatigue durability in potential applications, such as ocean engineering and civil engineering.

Keywords: Circular cylinder, direct numerical simulation, Lattice Boltzmann Method, Low-Reynold flow, vortex formation.

1. Introduction

In recent decades, research on the dynamic behavior of the flow through an array of tandem cylinders has attracted many researchers because of their various applications, such as heat exchanger tubes, bundled transmission lines, buildings, offshore risers, and even electronic chips on the mainboard. The related investigations are useful for better understanding and knowledge about fluid flow through such a system. Various arrangements of circular cylinders have been considered; however, the tandem configuration is more commonly used in the literature. In this configuration, it was found that the vortex originating from the upstream cylinder generally affects the downstream cylinder. Indeed, Zdravkovich *et al*. [1], Igarashi *et al*. [2,3], and Sumner *et al*. [4] comprehensively studied the fluid flow past the two identical cylinders. Zdravkovich [1], Igarashi *et al*. [2,3] reported the three following regimes of vortex formation, which was the function of the spacing between the cylinders (L/D): (i) the extended-body regime ($0.5 < L/D < 10$), (ii) the reattachment regime ($1.0 < L/D < 3.5$), and the co-shedding regime ($L/D > 3.5$), where D denotes a cylinder diameter.

The vortex shedding behind the downstream cylinder causes a vibration in the entire cylinder array or even structural damage. Arranging a flat plate behind a cylinder is reported to be a promising candidate to remove or at least reduce this vibration. Roshko *et al*. [5] investigated the periodic vortex formation suppression using a flat plate with a circular cylinder. It was found from this study that the critical gap spacing between the circular cylinder and detached flat plate is approximately 2.7 ($L_p/D \approx 2.7$). Additionally, the value of Strouhal number, $St = fD/U_\infty$, where f is the vortex shedding frequency from the cylinder, decreased with the presence of the flat plate. Apelt *et al*. [6] experimentally investigated the effect of a flat plate on the behavior of the fluid flow through a single cylinder at $Re = 10^4 \sim 5\times10^4$ and concluded that L_p (the length of the flat plate) is equal to D, the drag, and St was significantly decreased and reached the minimum value. Furthermore, Apelt and West [7] continuously experimentally studied the vortex formation of the flow through a cylinder and a flat plate. This author found that the vortex shedding disappeared, and the drag became constant when l/D (l is the gap from the upstreaming cylinder to the flat plate) was greater than 5. This demonstrated the effects of the flat plate on the vortex formation. Although some previous studies considered the effects of the flat plate on the vortex formation of the flow through a single cylinder, no research examines the dynamic

ISSN 2734-9381
https://doi.org/10.51316/jst.175.etsd.2024.34.3.6
Received: Dec 19, 2023; revised: Mar 28, 2024;
accepted: Mar 28, 2024

behaviors of the fluid flow through two tandem cylinders with the middle flat plate.

The objective of this study is to consider the flow through two tandem circular cylinders with a middle flat plate using the lattice Boltzmann Method in the Direct Numerical Simulation. The flat plate with its length as the function of the cylinder diameter at Re = 100, and L/D ranges from 3 to 10. Notably, the low Reynold number (Re) of 100 is to eliminate the effects of the turbulence flow [8].

2. Numerical Methodology

2.1. Lattice Boltzmann Method for Incompressible Flows

The fluid flow can be modeled by solving the governing equations. In the present study, the macroscopic behavior of the incompressible flow is governed by the continuity and Navier-Stokes equations. They are expressed in the following equation.

$$\begin{aligned} &\nabla \cdot u = 0, \\ &\frac{\partial u}{\partial t} + (u \cdot \nabla) u = -\nabla p + \frac{1}{Re} \nabla^2 u, \end{aligned} \tag{1}$$

where $\boldsymbol{u}$, p, and t are the local velocity vector, pressure, and time, respectively. Re stands for the Reynolds number of $Re = U_\infty D/\nu$ with the reference velocity U_∞, the characteristic length D, and the kinematic viscosity ν of fluid. Equation (1) are solved using the lattice Boltzmann Method (LBM) on a uniform Cartesian grid.

Let us consider the discretization of the two-dimensional D2Q9 lattice model with nine velocities. A distributional population f_i is involved in computing the velocity field. Unit space lattice (Δx) is used to model the location of the population in the LBM method. Particles distribute on a fixed Cartesian square lattice along the links i = 0, ..., 8 with lattice velocity $c_i = (c_{xi}, c_{yi})$. Values of those are defined in the following equation [9].

$$\boldsymbol{c}_i = \begin{cases} (0,0) & i = 0 \\ (0,\pm 1)c,\ (\pm 1,0)c & i = 1,2,3,4 \\ (\pm 1,\pm 1)c & i = 5,6,7,8 \end{cases} \tag{2}$$

where $c = \Delta x / \Delta t$ represents the lattice speed, Δx is the lattice length, and Δt is the constant time step. The most important variable in the LBM is the particle distribution function (PDF) $f_i(x,t)$, which indicates the chance of meeting a particle with a velocity c_i at the spatial point and time t. The state of the fluid is updated by computing the particle distribution function using the discrete Boltzmann equation shown below.

The macroscopic variables (the fluid density ρ and fluid velocity $\boldsymbol{u}$) in LBM are obtained from populations using its moments, as shown in the following equation.

$$\rho = \sum\nolimits_i f_i, \quad \rho \boldsymbol{u} = \sum\nolimits_i c_i f_i \tag{3}$$

The Bhatnagar-Gross-Krook collision model [17] with a single relaxation time is used. The framework of the numerical procedure is divided into two key parts. Firstly, a local process called the collision process is governed by following equation.

$$f_i^* = f_i - \frac{1}{\tau}(f_i - f_i^{eq}), \tag{4}$$

where the superscript "*" indicates the post-collision state and is the equilibrium state of populations given by following equation.

$$f_i^{eq} = \rho w_i \left[1 + 3c \cdot \boldsymbol{u} + \frac{9}{2}(c \cdot \boldsymbol{u})^2 - \frac{3}{2} \boldsymbol{u} \cdot \boldsymbol{u} \right] \tag{5}$$

where the coefficient w_i for the D2Q9 model is:

$$w_i = \begin{cases} 4/9 & i = 0, \\ 1/9 & i = 1,2,3,4, \\ 1/36 & i = 5,6,7,8 \end{cases}$$

The kinematic viscosity is linked to the relaxation time by the following formula by the following equation.

$$\nu = c_s^2 \left(\tau - \frac{\Delta t}{2} \right) \tag{6}$$

where c_s^2 is the lattice sound speed. The pressure field may be calculated using the state equation for an ideal gas, $p = \rho c_s^2$

The relaxation time is related to the fluid kinematic viscosity ν, as shown in the following equation.

$$\tau = \frac{1}{2} + \frac{\nu}{c_s^2} \tag{7}$$

Next, the streaming process is implemented to transport post-collision populations from the particle at location x to neighboring particles at location $x + c_i$ [9]. This computation procedure is governed by the following equation.

$$f_i(x + c_i \Delta t, t + \Delta t) = f_i^*(x,t), \tag{8}$$

In (8), the time step (Δt) sets as a unity in the lattice unit. This process is implemented on the lattice link between two adjacent fluid particles. It is well understood that the only condition one must satisfy in numerical simulations of incompressible flow is Ma<<1, where $Ma = U_\infty / c_s$ is the Mach number. As a

result, the density is approximately constant, and the density fluctuation is neglected. For particles representing the rigid object, the streaming process is not performed. The interpolated bounce-back (IBB) method [10-11] is proposed to replace the streaming procedure. When a fluid particle located at x_f has a lattice link along a $\bar{i}$-direction prevented by a solid particle located at x_s, the unknown distribution function along the opposite direction i is computed using a linear interpolation function. This interpolation uses the post-collision distribution function of itself and adjacent fluid particles located at x_{ff} in the i-direction. This numerical procedure is formulated by following equation.

$$f_i(x_f, t+\Delta t) = \begin{cases} 2qf_i^*(x_f,t) + (1-2q)f_i^*(x_{ff},t) & q \le \frac{1}{2} \\ \frac{1}{2q}f_i^*(x_f,t) + \frac{2q-1}{2q}f_i^*(x_{ff},t) & q \ge \frac{1}{2} \end{cases} \quad (9)$$

where $q = |x_f - x_i|/|x_f - x_s|$ is a spatial ratio with x_i indicating the intersection point between the lattice link and boundary curve, the normalized output macroscopic variables in LBM are expressed by $x^* = x/D$, $\boldsymbol{u}^* = \boldsymbol{u}/U_\infty$, $t^* = tU_\infty/D$, $p^* = (p-p_0)/(\rho U_\infty^2)$ and $Re = DU_\infty/\nu$, where p_0, U_0, D, and ν denote reference pressure, reference velocity U_0, the characteristic length D, and kinematic viscosity ν in lattice unit. Total fluid forces acting on the 2D rigid body's surface (F (F_x, F_y)) are computed by the momentum exchange method [12] on the boundary cell layer. The global hydrodynamic coefficients, such as lift and drag coefficients, pressure coefficient, Strouhal number, mean drag coefficient, and root-mean-square value of lift coefficient, are accordingly computed by following equation.

$$C_D = \frac{F_x}{\frac{1}{2}\rho U_\infty^2 D_2}, \quad C_L = \frac{F_y}{\frac{1}{2}\rho U_\infty^2 D_2},$$
$$C_P = \frac{p-p_\infty}{\frac{1}{2}\rho U_\infty^2}, \quad St = \frac{f \cdot D_2}{U_\infty}, \quad (10)$$
$$\bar{C}_D = \frac{1}{N}\sum_1^N C_D, \quad C_L' = \sqrt{\frac{1}{N}\sum_1^N (C_L - \bar{C}_L)^2}$$

where N is the number of instants of a time history data.

2.2. Numerical Setup and Validation

The schematic diagram of a numerical model is shown in Fig. 1. The viscous incompressible fluid flows over two tandem circular cylinders with a middle flat plate. Boundary conditions (BC) used in this numerical model are also shown in Fig. 1. A no-slip condition was applied on cylinder surfaces. A constant velocity condition ($u = U_\infty$, $v = 0$) was used for the inlet, and the free-slip BC was applied at the upper and lower boundaries of the computational domain. An outflow BC $\partial u/\partial x = \partial v/\partial x = 0$ was adopted at the outlet boundary. The upstream cylinder (C1, hereafter) was located at the coordinate origin, and the downstream cylinder (C2, hereafter) was mounted at the distance L from C1. The middle flat plate has the length L_p and the thickness t_p, and it was mounted at the distance l from the upstream cylinder, as shown in Fig. 1.

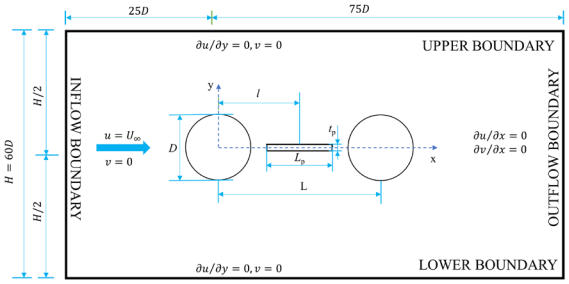

Fig. 1. Schematic of the numerical model and boundary conditions

Additionally, the computational domain size $100D \times 60D$ was used. In this regard, the blockage ratio ($B = D/H$, where $H = 60D$ is the width of the computational domain) is less than 2%, satisfying the sufficiently required blockage ratio threshold of 6% [13]. The inflow boundary is located upstream at $25D$ to the center of C1, and the outflow boundary is located downstream at $75D$ to the center of C1. The reference velocity is set as $U_\infty = 0.1$ in the lattice unit at the inflow and lower boundaries, corresponding to the non-dimensional time step of $\Delta t^* = \Delta t U_\infty/D = 0.001$ to capture fully developed flow patterns for all cases. Therefore, two-dimensional simulations are performed for a non-dimensional time of $t^* = N \cdot \Delta t^* = 200$. This nondimensional time corresponds to approximately 20 periods of Karman vortex shedding, sufficient to reach the asymptotic wake state.

A framework of topology-confined block refinement was used based on the block-structured grids reported in Duong's study [14]. The computational domain was partitioned into areas of different grid sizes, called cube-shaped blocks. This spatial difference is characterized by an indicator called refinement level (k) ranging from 0 to $k = m-1$, where m is the number of the expected refinement level. k increases from the confined flow region near the solid bodies to far-field regions. The uniform Cartesian grid (called cells) is distributed in each block to solve the macroscopic variables in LBM. The detailed algorithm was referred to Ref. [14].

The mesh convergence was implemented by changing the number of cells in each block (*Ncell*). In this study, *Ncell* varied from 40 to 80, as shown in

Fig. 2. It was found from this figure that relative deviations of the hydrodynamic coefficients and the Strohal number compared to those of the finest mesh (*Ncell* = 80) are 1.78%, 2.06%, 1.44%, and 0.38% for $\bar{C}_D$; 4.16%, 4.78%, 0.72%, and 8.07% for C'_L; and 1.18%, 0.59%, 0.59%, 0% for *St,* respectively. Based on these results, the maximum deviation is less than 5% at *Ncell* = 50. Therefore, this mesh model was used for further computations in this study.

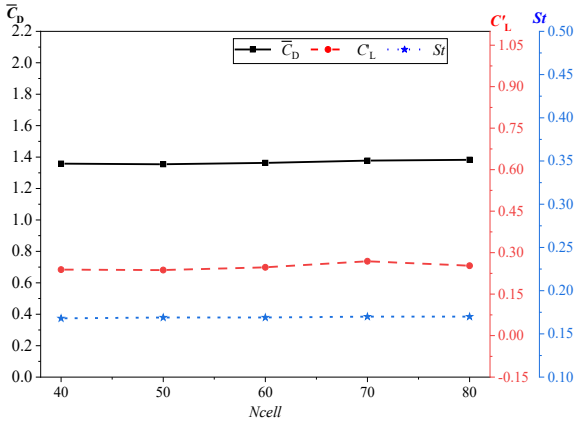

Fig. 2. Mesh convergence tests for various hydrodynamic coefficients

Table 1. A code validation for the flow through a single circular cylinder at *Re* = 100

Authors	$\bar{C}_D$	C'_L	*St*
Williamson [15]	-	-	0.164
Chen *et al*. [16]	1.337	0.23	0.163
Present work	1.348	0.236	0.169
Maximum Deviation (%)	0.82	2.61	3.68

Table 2. A code validation for the flow through two tandem circular cylinders at *L*/*D* = 4 and *Re* = 100

Authors	$\bar{C}_{D1}$	$\bar{C}_{D2}$	$\bar{C}_{L1}$	$\bar{C}_{L2}$	*St*
Jiang *et al*.	1.28	0.723	0.464	1.39	0.15
Sharma *et al*.	1.28	0.71	0.44	1.39	0.148
Mussa *et al*.	1.3	0.73	0.46	1.44	0.148
Present work	1.29	0.71	0.46	1.39	0.151
Maximum Deviation (%)	0.78	2.74	4.55	3.47	2.03

First, the numerical model was validated for the important hydrodynamic coefficients ($\bar{C}_D$, C'_L, and *St*) of the flow through a single circular cylinder at *Re* = 100, as shown in Table 1. The numerical results were compared with those obtained by Williamson [15] and Chen *et al*. [16]. As a result, the maximum deviation is less than 4% compared to Chen's results. It was also valid when compared with the *St* values obtained by Williamson [15].

Second, the numerical model was also validated for a case of two tandem circular cylinders, as shown in Table 2 In this regard, the important hydrodynamic coefficients for the upstream cylinder ($\bar{C}_{D1}$, C'_{L1}), the downstream cylinder ($\bar{C}_{D2}$, C'_{L2}), and the Strouhal number of the upstream and downstream cylinder (St_1 and St_2) were determined at *L*/*D* = 4 and *Re* = 100. The numerical results were compared with those obtained by Jiang *et al*. [17], Sharman *et al*. [18], and Mussa *et al*. [19]. Consequently, the maximum deviation is less than 4.6%. In summary, this numerical model was well-validated with adaptively high accuracy. Thus, it can be used for further computations in the present study.

3. Results and Discussions

Fig. 3 and Fig. 4 show the flow vorticity field for various cylinder spacings *L*/*D* of 3, 5, 7, and 10. Two testing cases were considered, i.e., without the flat plate as shown in Fig. 3 and with the flat plate as shown in Fig. 4. First, for a case without a flat plate considered, three regimes of vortex formation, i.e., overshoot, reattachment, and co-shedding, were observed. These regimes depend significantly on the cylinder spacing. At a small *L*/*D* shown in Fig. 3(a), the fluid flow is able to move over both circular cylinders. This is because the small spacing between two cylinders limits the development or oscillation of the downstream wake when the flow moves through the upstream cylinder. Therefore, the overshoot regime is formed. However, the downstream wake of the upstream cylinder can oscillate when the spacing is large enough, *L*/*D* = 5 and 7, as shown in Fig. 3(b) and Fig. 3(c), respectively. This wake can touch the second cylinder; hence, the reattachment regime forms in this case. Moreover, the co-shedding regime forms when the spacing between cylinders further increases. In this case, vortices are created at the back of the first cylinder and detach periodically from either side of this cylinder, forming a Kármán vortex street. This result is in line with the results reported by Zdravkovich *et al*. [1]. Again, this result indicates the confidence of the numerical model used in the present study.

However, the vortex regimes mentioned previously can be changed with the presence of the flat plate at the threshold values of *L*/*D*. Indeed, at *L*/*D* = 3 and 10, the vortex regimes of overshoot and co-shedding exist regardless of the presence of the flat

plate. The reattachment regime becomes quasi-cosedding at the threshold values of $L/D = 5$ and 7. Moreover, the two-layer vortices also become the primary ones forming in the wake flow, as shown in Fig. 4(b) and 4(c). Notably, the name of quasi-coshedding was first referred to Duong *et al.* [14]. These results imply that changing vortex regimes of the flow through two tandem circular cylinders may result in the variation of the flow characteristics. This is clearly shown in the next section with the quantitative results.

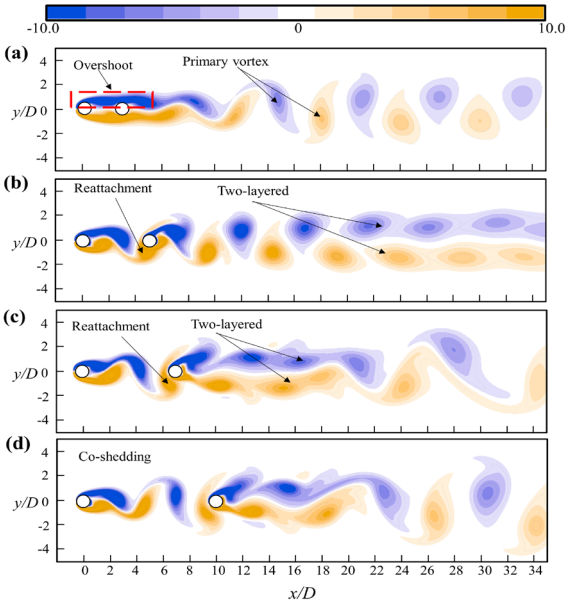

Fig. 3. Flow vorticity field for various cylinder spacings without flat plate: a) $L/D = 3$, b) $L/D = 5$, c) $L/D = 7$, and d) $L/D = 10$

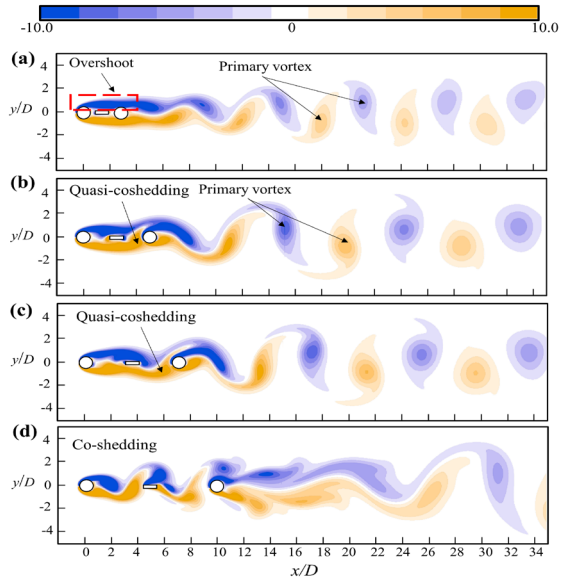

Fig. 4. Flow vorticity field for various cylinder spacings with flat plate: a) $L/D = 3$, b) $L/D = 5$, c) $L/D = 7$, and d) $L/D = 10$

To quantitatively examine the flow characteristics, variations of hydrodynamic coefficients and the Strouhal number for two cases with and without flat plate were calculated as a function of L/D, as shown in Fig. 5 and Fig. 6. These coefficients are also compared with those of the single circular cylinder to validate the asymptotic results (dot line on the left figures).

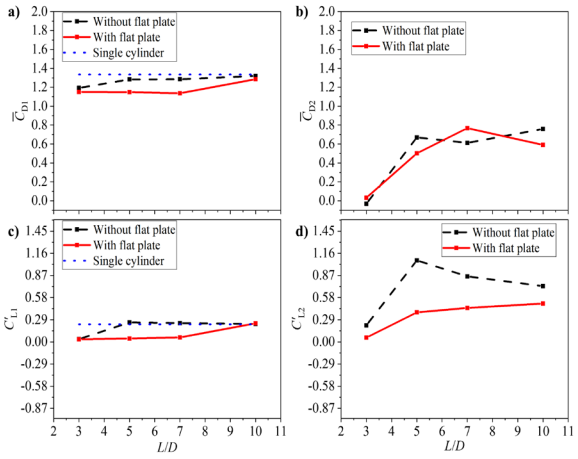

Fig. 5. Variations of $\overline{C}_D$, C'_L with L/D for the upstream cylinder C1 (left) and the downstream cylinder C2 (right)

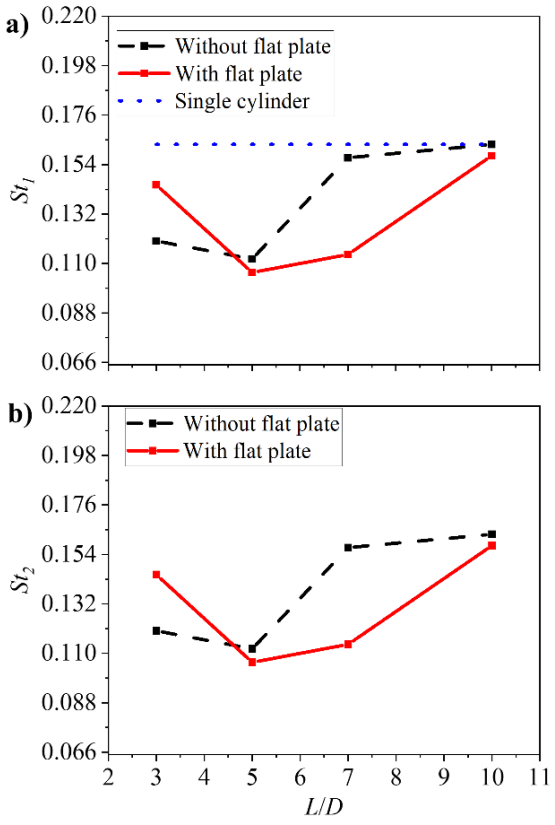

Fig. 6. Variations of St with L/D for the upstream cylinder C1 (left) and the downstream cylinder C2 (right)

It was seen that the hydrodynamic coefficients and the Strohal number generally decrease when the flat plate is mounted in the middle of two cylinders apart from the *St* at L/D=3. It means the frequency of the vortex formation or the oscillation influence on the cylinder system can be reduced using the middle flat plate.

Fig. 5 and Fig. 6 also indicate the asymptotic results of hydrodynamic coefficients and Strouhal number when the cylinder spacing becomes large enough. The parameters tend to increase and approach a plateau value (a blue-dot horizontal line). At this point, the mutual interaction between cylinders is low, and the flow through the upstream cylinder becomes relatively stable before it moves through the downstream cylinder. This is valid for both cases with and without the flat plate. However, the asymptotic progress is lower when the flat plate is mounted between cylinders, as shown in Figs. 5(a), 5(c), and Fig. 6(a). This again indicates the limitation of vortex formation with the presence of the flat plate. This effect is predicted to become more significant if the size of the flat plate increases, as shown in the next paragraphs.

To visualize the effects of the flat plate size, Fig. 7 shows the vorticity field for the following six cases: without a flat plate, L_p/D=0.1, 0.5, 1.0, 1.5, and 2.0, corresponding to Figs.7(a) to 7(f). It was found that the pattern of vortex formation changes at the threshold value of plate size. With a small size (L_p/D=0.1), the vortex regime of reattachment with two-layered wake flow forms resembling no flat plate case. When L_p/D gradually increases, the effects of the flat plate become more significant, the reattachment vortex reduces, and the primary vortex appears at the wake flow instead of the two-layered wake. This is shown in Fig.7(c) and 7(d). At a larger L_p/D up to 1.5 and even 2.0, the vortex regime changes from the reattachment to the quasi-coshedding and overshoot regime. In this regard, the flat plate is large enough that the oscillation of wake flow through the upstream circular cylinder is limited or omitted completely at the largest size.

Fig. 8 shows the variations of hydrodynamic coefficients with L_p/D for both the upstream cylinder (left) and the downstream cylinder (right). The green dash-dot line indicates the case without the flat plate, and the blue dot line indicates the results of the single circular cylinder. Consequently, hydrodynamic coefficients and the Strouhal number generally decrease with increasing the flat plate size. This effect can be seen more clearly in the downstream cylinder with the higher slope of $\overline{C}_{D2}$, C'_{L2} compared with $\overline{C}_{D1}$, C'_{L1}. Additionally, they are frequently lower than single circular cylinders, as shown in Fig.8 (left). It is also valid for the lift and drag coefficients compared to no flat plate.

However, this trend changes for the Strouhal number, as shown in Fig. 9. The St_1 decreases when L_p/D is less than 1.0, but it increases at higher L_p/D. This is also valid for the St_2, but the minimum *St* obtains at L_p/D=1.5. This also accounts for the change of vortex regime in the previous section and provides good guidelines for ocean engineering.

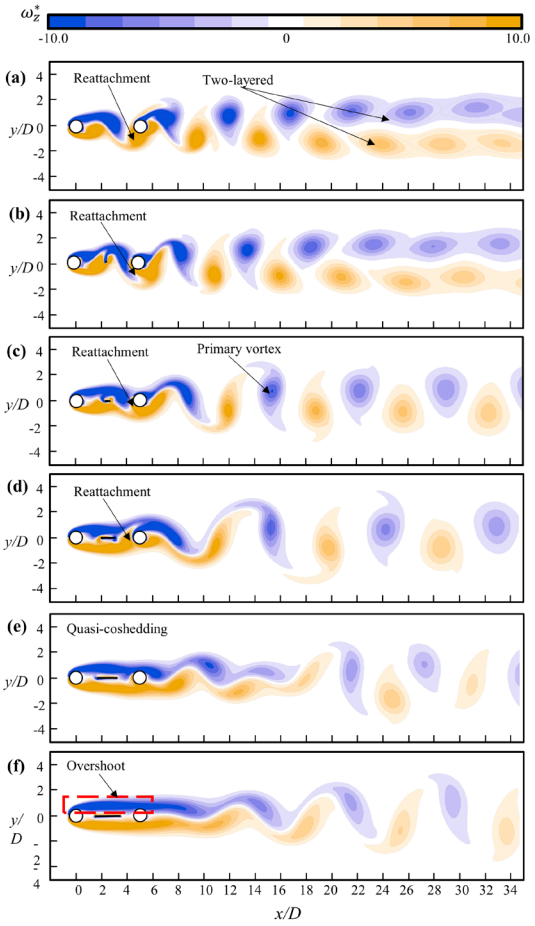

Fig. 7. Vorticity field as a function of the flat plate size at L/D = 5: a) without flat plate, b) L_p/D=0.1, c) L_p/D=0.5, d) L_p/D=1.0, e) L_p/D=1.5, and f) L_p/D=2.0

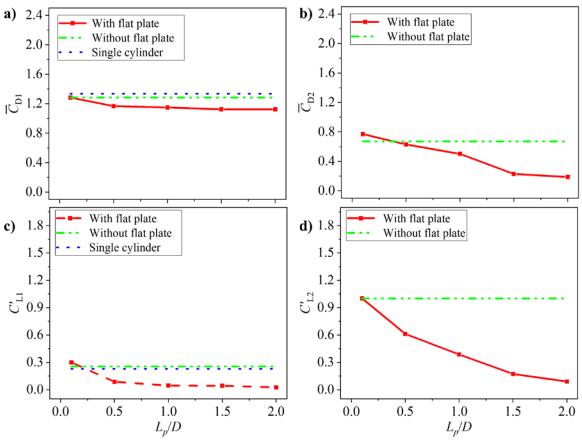

Fig. 8. Variations of $\overline{C}_D$, C'_L with L_p/D for upstream cylinder C1 (left) and downstream C2 (right)

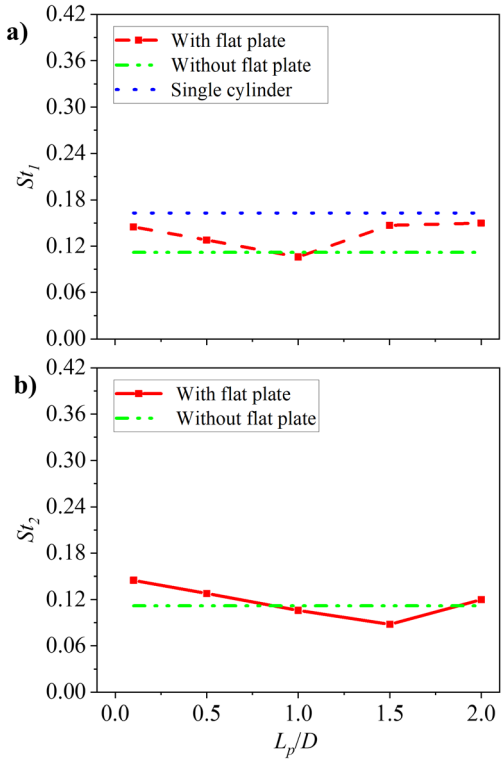

Fig. 9. Variations of St with L_p/D for upstream cylinder C1 (left) and downstream C2 (right)

4. Conclusion

The fluid flow through two tandem cylinders with the middle flat plate has been numerically investigated using the Lattice Boltzmann Method in the Direct Numerical Simulation. The research aimed at the effects of the middle flat plate was examined. Consequently, the results obtained can be drawn as follows:

- The numerical model was well-validated compared to the literature results for single circular cylinders and two tandem cylinders without flat plates;

- The dynamic behaviors of the fluid flow through two tandem cylinders with the middle flat plate were first examined in this study;

- The pattern of vortex formation is affected significantly by the presence of the middle flat plate, and it changes at the threshold value of plate size;

- Hydrodynamic coefficients and the Strouhal number generally decrease with the increase in flat plate size.

These results help to reduce the losses caused by the vortex formation and increase the fatigue durability in potential applications, such as ocean engineering and civil engineering. Moreover, further studies can be performed to optimize the size and position of the flat plate along with the other important parameters, such as the cylinder spacing, Reynold number, etc.

Acknowledgments

This research is funded by Vietnam National Foundation for Science and Technology Development (NAFOSTED) under grant number 107.03-2021.37.

References

[1] M. Zdravkovich, Review of flow interference between two circular cylinders in various arrangements, Trans. ASME J. Fluids Eng, vol. 99, no. 4, pp. 618-633, Dec. 1977. https://doi.org/10.1115/1.3448871

[2] T. Igarashi, Characteristics of the flow around two circular cylinders arranged in tandem: 2nd report, unique phenomenon at small spacing, Bulletin of JSME, vol. 27, no. 233, pp. 2380-2387, 1984. https://doi.org/10.1299/jsme1958.27.2380

[3] T. Igarashi, Characteristics of the flow around two circular cylinders arranged in tandem: 1st report, Bulletin of JSME, vol. 24, no. 188, pp. 323-331, 1981. https://doi.org/10.1299/jsme1958.24.323

[4] D. Sumner, Two circular cylinders in cross-flow: a review, Journal of Fluids Structures, vol. 26, no. 6, pp. 849-899, Aug. 2010. https://doi.org/10.1016/j.jfluidstructs.2010.07.001

[5] A. Roshko, On the drag and shedding frequency of two-dimensional bluff bodies, no. NACA-TN-3169, Jul. 1954.

[6] C. J. Apelt, G. S. West, and A. A. Szewczyk, The effects of wake splitter plates on the flow past a circular cylinder in the range $10^4 < R < 5 \times 10^4$, Journal of Fluid Mechanics, vol. 61, no. 1, pp. 187-198, Oct. 1973. https://doi.org/10.1017/S0022112073000649

[7] C. J. Apelt and G. S. West, The effects of wake splitter plates on bluff-body flow in the range $10^4 < R < 5 \times 10^4$. Part 2, Journal of Fluid Mechanics, vol. 71, no. 1, pp. 145-160, Sep. 1975. https://doi.org/10.1017/S0022112075002479

[8] P. Vorobieff, D. Georgiev, and M. Ingber, Onset of the second wake: dependence on the Reynolds number, Physics of Fluids, vol. 14, no. 7, pp. 53-56, Jul. 2002. https://doi.org/10.1063/1.1486450

[9] T. Krüger *et al.*, The lattice Boltzmann Method, Springer International Publishing, vol. 10, no. 978-3, pp. 4-15, 2017.

[10] M. H. Bouzidi, M. Firdaouss, and P. Lallemand, Momentum transfer of a Boltzmann-lattice fluid with boundaries, Physics of Fluids vol. 13, no. 11, pp. 3452-3459, Nov. 2001. https://doi.org/10.1063/1.1399290

[11] A. J. Ladd, Numerical simulations of particulate suspensions via a discretized Boltzmann equation. Part 1. Theoretical Foundation, vol. 271, pp. 285-309, Jul. 1994. https://doi.org/10.1017/S0022112094001771

[12] Y. Chen, Q. Cai, Z. Xia, M. Wang, and S. Chen, Momentum-exchange method in lattice Boltzmann simulations of particle-fluid interactions, Physical Review E, vol. 88, no. 1, pp. 013303, Jul. 2013. https://doi.org/10.1103/PhysRevE.88.013303

[13] Q. Zheng and M. M. Alam, Intrinsic features of flow past three square prisms in a side-by-side arrangement, Journal of Fluid Mechanics, vol. 826, pp. 996-1033, Sep. 2017. https://doi.org/10.1017/jfm.2017.378

[14] V. D. Duong, V. D. Nguyen, V. T. Nguyen, and I. L. Ngo, Low-Reynolds-number wake of three tandem elliptic cylinders, Physics of Fluids, vol. 34, no. 4, pp. 043605, Apr. 2022. https://doi.org/10.1063/5.0086685

[15] C. H. K. Williamson, Vortex Dynamics in the Cylinder Wake, Annual Review of Fluid Mechanics, vol. 28, pp. 477-539, Jan. 1996. https://doi.org/10.1146/annurev.fluid.28.1.477

[16] S. Chen and G. D. Doolen, Lattice Boltzmann method for fluid flows, Annual Review of Fluid Mechanics, vol. 30, no. 1, pp. 329-364, Jan. 1998. https://doi.org/10.1146/annurev.fluid.30.1.329

[17] R. Jiang, J. Lin, and X. Ku, Numerical predictions of flows past two tandem cylinders of different diameters under unconfined and confined flows, Fluid Dynamics Research, vol. 46, no. 2, pp. 025506, Feb. 2014. https://doi.org/10.1088/0169-5983/46/2/025506

[18] B. Sharman, F.-S. Lien, L. Davidson, and C. Norberg, Numerical predictions of low Reynolds number flows over two tandem circular cylinders, International Journal for Numerical Methods in Fluids, vol. 47, no. 5, pp. 423-447, Feb. 2005. https://doi.org/10.1002/fld.812

[19] A. Mussa, P. Asinari, and L.-S. Luo, Lattice Boltzmann simulations of 2D laminar flows past two tandem cylinders, Journal of Computational Physics, vol. 228, no. 4, pp. 983-999, Mar. 2009. https://doi.org/10.1016/j.jcp.2008.10.010